

Journal of Optoelectronical Nanostructures



Volume 10, Issue 3, Autumn 2025, Page 21-37

Research Paper (Pape Type)

Enhancing CIGS Solar Cell Efficiency through Gold, Silver, and Aluminum Plasmonic Nanostructures

Marzieh Akbari¹, Fatemeh Dabbagh Kashani^{*,1}, Seyyed Mohammad Mirkazemi²

- ¹ School of Physics, Iran University of Science and Technology, Tehran, Iran
- ² Ceramic group, School of metallurgy and Materials Engineering, Iran University of Science and Technology, Tehran, Iran

Received: 2025.05.17 Revised: 2025.08.20 Accepted: 2025.08.20 Published: 2025.11.30

Use your device to scan and read the article online



Keywords:

Chalcopyrite photovoltaic cells, FDTD simulation method, Noble metalbased plasmonic effects, Optical and Electrical performance analysis Abstract Plasmonic nanostructures offer significant benefits for enhancing solar cell performance by improving light absorption, charge carrier generation, exciton separation. and reducing recombination. However, challenges such as current reduction must be addressed through careful material selection and optimization. CIGS-based solar cells, known for their cost-effectiveness and superior efficiency compared to silicon-based cells, are further improved with plasmonic nanostructures. This study investigates the impact of plasmonic effects on CIGS solar cells, showing that the efficiency depends on the Dimensions, Geometry, and arrangement of the nano elements. Simulations of optical and electrical properties, including absorption curves and current-voltage characteristics, reveal that Sample 5 (a solar cell with gold spherical elements at the top of the absorber layer and gold cubic elements at the bottom), which combines two plasmonic nanostructure series, achieves the highest efficiency increase of 25.13%. However, a single plasmonic nanostructure in the active layer offers similar efficiencies with greater costeffectiveness and simplified manufacturing. findings highlight the potential of single-series plasmonic nanostructures for advancing solar technology while ensuring practical feasibility in production.

*Corresponding author: Fatemeh Dabbagh Kashani

Address: School of Physics, Iran University of Science and Technology, Tehran, Iran. Enhancing CIGS Solar Cell Efficiency through Gold, Silver, and Aluminum Plasmonic Nanostructures. **Journal of Optoelectronical Nanostructures.** 2025; 10(3): 21-37.

Email: f_dk@iust.ac.ir

DOI: https://doi.org/10.71577/jopn.2025.1207117

1. Introduction

Copper indium gallium selenide (CIGS) solar cells are highly efficient and offer promising potential for cost-effective production. However, enhancing their performance remains essential to keep pace with rising energy demands [1-6]. One effective approach to increasing CIGS solar cell efficiency involves incorporating plasmonic nanoparticles, often made of metals like gold (Au) and silver (Ag). These nanoparticles amplify light absorption through localized surface plasmon resonance (LSPR), which generates resonant electron density waves and increases light scattering within the solar cell structure [7-12]. By embedding plasmonic nanoparticles into CIGS cells, the optical path length of incoming light is extended, intensifying absorption in the active layer through scattering and near-field effects that concentrate light within the semiconductor material [13,14]. Research has shown that plasmonic nanostructures efficiently absorb a broad range of light wavelengths and are cost-effective to manufacture using adjustable parameters such as size, shape, material composition, and location within the cell structure [9], [14, 15]. The optical properties of these nanoparticles are tunable, which allows for a high degree of customization in the design of solar cells. Gold and silver are particularly advantageous due to their high dense population of conduction band electrons, Intense localized surface plasmon oscillations, wide spectral absorption range, and stability, making them ideal candidates for light management in solar cells [9], [13-15]. Moreover, careful selection of nanoparticle size, shape, and distribution enables optimization of light-trapping effects. Studies demonstrate that specific nanoparticle shapes, such as spherical or cylindrical, yield distinct light-trapping and scattering behaviors, which can be engineered to further boost efficiency in CIGS solar cells. Such enhancements allow more light to be absorbed and converted, elevating the overall power conversion efficiency compared to cells without these enhancements [14], [16-18].

This study examines innovative methods to optimize light absorption and conversion efficiency by integrating Ag, Au, and Al plasmonic nanocubics and nanospheres with various sizes, occupancy factors, and distributions into CIGS solar cells (Figure 1). The examined samples of permutations combining plasmonic elements in cubic and spherical shapes with the highest efficiency (based on the results of our previous studies) in different positions of the absorber layer are presented in Table 1. Notably, simulations indicated that gold (Au) and silver (Ag) nanostructures generally yielded higher efficiency enhancements compared to aluminum (Al). This is consistent with their superior plasmonic properties, including higher free electron densities and lower optical

losses in the visible and near-infrared spectrum relevant to CIGS absorption, compared to Al which tends to exhibit higher ohmic losses. Trough theoretical analyses, we investigate the mechanisms by which these nanostructures improve light absorption and energy conversion, alongside recent advances in the fabrication and integration of plasmonic nanostructures in CIGS solar cells. The samples are as follows:

- Sample 1: A solar cell with spherical elements at the bottom of the absorber layer and cubic elements in the middle of the absorber layer.
- Sample 2: A solar cell with spherical elements at the bottom of the absorber layer and cubic elements at the top of the absorber layer.
- Sample 3: A solar cell with spherical elements in the middle of the absorber layer and cubic elements at the bottom of the absorber layer.
- Sample 4: A solar cell with spherical elements in the middle of the absorber layer and cubic elements at the top of the absorber layer.
- Sample 5: A solar cell with spherical elements at the top of the absorber layer and cubic elements at the bottom of the absorber layer.
- Sample 6: A solar cell with spherical elements at the over absorber and cubic elements in the middle of the absorber layer.

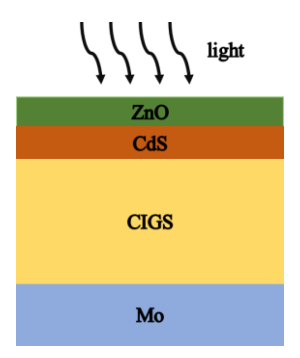


Fig. 1. CIGS device configuration

Table 1 lists the individual plasmonic nanostructures (shape, size, material, location) that yielded the highest efficiency when incorporated into the baseline solar cell structure during parameter sweeps.

Table 1. Lists	of best samp	les in present	of nanostructures

Shape	Size	Material	O.F.	Location	Efficiency
	50	Al	0.16	Bottom	22.65%
Spherical	200	Ag	0.64	Middle	22.99%
	200	Au	0.64	Top	25.28%
	200	Ag	0.64	Bottom	22.17%
Cubic	100	Au	0.16	Middle	22.94%
	100	Au	0.16	Top	25.61%

2. DEVICE STRUCTURE AND SIMULATION METHODOLOGY

To optimize Photovoltaic efficiency and gain insights into their functional characteristics, computational simulations play an indispensable role [19-20]. They offer an economical and efficient way to evaluate different design setups. forecast functional behavior across various conditions, and investigate methods to improve performance. Developing a robust model, understanding parameter sensitivity, and validating results with experimental data are essential steps in this process, though simulations can be complex and computationally intensive. Despite these challenges, numerical simulations remain vital for development and analysis of solar cells, enabling performance optimization and guiding the development of high-efficiency solar energy systems. Light-based simulations, including those using the Finite-Difference Time-Domain approach [21,22], allow us to study the interaction of light with photovoltaic cell. This method involves discretizing the cell structure, refreshing electromagnetic fields values over time, and implementing boundary conditions iteratively to compute Maxwell's equations. FDTD analysis effectively captures the absorption of light, reflection, and transmission within the cell, offering valuable insights for optimizing design and enhancing cell efficiency.

Electrical simulations, whereas, use drift-diffusion equations to analyze charge carrier behavior within semiconductor materials. By modeling carrier transport, recombination, and other electrical dynamics, these simulations enable researchers to explore the performance of photovoltaic devices across different operational conditions and to optimize electrical efficiency through numerical solutions of the drift-diffusion equations [23]. The next sections aim to explore optoelectrical characterizations of photovoltaic devices, focusing on scenarios with and without plasmonic elements. Key parameters examined include absorption, and photovoltaic conversion efficiency. These analyses provide a comprehensive understanding of the factors that influence solar cell efficiency and inform the design choices that drive optimal energy conversion performance.

To compute absorption amount per volume unit, we can use the divergence of the Poynting vector. However, direct calculations of the divergence often exhibit significant numerical sensitivity, making precise results challenging to obtain [24]. A more numerically stable alternative formulation is available, which can enhance the accuracy of these computations. This revised equation can be applied to more reliably determine the absorption distribution within the material [7]

$$Pabs = -0.5\omega |E|^2 imag(\varepsilon)$$
(1)

Where Pabs is absorption power, ω is the angular frequency, E is the magnitude of the electric field and ϵ is permittivity, representing losses due to absorption. The photovoltaic conversion efficiency (η) reflects its capability to transform incident solar radiation into practical electrical power. This metric represents the proportion of electrical power produced by the solar cell relative to the power of the incident sunlight, offering a key indicator of the cell's effectiveness in converting solar energy into electricity [25].

$$\eta = \frac{FF \times V_{\infty} \times J_{sc}}{S_{AM1.5G}} \tag{2}$$

The efficiency η of a solar cell is influenced by several factors. Fill Factor (FF) evaluates the "squareness" of the current-voltage (IV) diagram in the cell's electrical property characterization, indicating how closely the cell's actual power output approaches its theoretical maximum. Open-Circuit Voltage (Voc) which is the maximum voltage available from the solar cell when there is no external load (open circuit). Short-Circuit Current (Jsc) representing the peak current flowing when the device's terminals are shorted (zero external resistance). The overall efficiency formula incorporates these factors along with the incident power under standard testing conditions, specifically from the AM1.5G solar spectrum model, which corresponds to an irradiance of 100 mW/cm². In this study, we investigate a CIGS (Copper Indium Gallium Selenide) thin-film solar cell (SC) enhanced with silver, gold, and aluminum nanostructures, which are evenly distributed across its active layer. Using Finite-Difference Time-Domain (FDTD) simulations, we analyze the light absorption behavior of this structure. As shown in Figure 1, the nanostructures are arranged in a periodic configuration. The CIGS layer, serving as the absorber in the simulation, is a p-type semiconductor and the primary site of the solar energy conversion effect. This effect facilitates the conversion of photon energy into electrical current. The junction is formed by a buffer layer composed of p- and n-type CdS and Cu (In, Ga) Se₂. Additionally, a transparent conductive oxide (TCO) layer, typically zinc oxide (ZnO), functions as the window layer, allowing light to enter the cell and facilitating electron transport out of the device. Zinc oxide is transparent to incoming light and plays a critical role in current transmission. Silver (Ag) and molybdenum (Mo) serve as the front and back electrodes, respectively. These electrodes are responsible for collecting the electrons generated by the solar cell. The buffer layer, along with the front contact layers, contributes to high cell efficiency by promoting effective energy transfer and collection. The optoelectrical variables required for the simulation are sourced from relevant literature [26-28].

Table 2. Lists the optoelectrical characteristics of the simulated structure [26-28]

	Thickness			_			
Material	x- axis (nm)	y- axis (nm)	z- axis (nm)	Doping Type	Doping(cm ⁻³)	Permittivity(ϵ)(F/m)	
ZnO	500	500	80	n-type	1 e+20	9	
CdS	500	500	60	n-type	1 e+18	10	
CIGS	500	500	1000	p- type	1 e+16	13.6	
Mo	500	500	500	-	-	=	

In this study, a plasmonic-free solar cell was used as a baseline to evaluate the impact of plasmonic elements on CIGS solar cell performance. The photovoltaic devices were simulated by employing the AM 1.5G solar spectrum at a temperature of 300K and irradiated by a broadband plane wave illumination source spanning light wavelengths covering 350–1150 nm. To compare the effectiveness of plasmonic-enhanced designs, various configurations using silver, gold, and aluminum nanostructures were evaluated. The analysis focused on three main structural adjustments: positioning the nanostructures at different depths within the absorbent layer (bottom, middle, or top), changing their size, altering the surface area they occupy (Occupied Surface, O.F) and the shape of plasmonic nanostructures. This systematic approach allowed for a detailed comparison of how each structural parameter influences the solar cell's absorption and overall efficiency.

Designing and characterizing solar cells requires both optical and electrical simulations. Using the Finite-Difference Time-Domain (FDTD) method, optical simulations analyze factors like carrier type and concentration across cell layers, recombination rates, and other parameters critical for solar cell performance, including light absorption, efficiency.

In the absorption calculation, key steps include adjusting the layout of cell layers, setting up the modeled region and boundary conditions, defining the

mesh size, and computing Maxwell's formulas using the FDTD approach within the Yee cell structure [29].

$$\frac{\partial \vec{D}}{\partial t} = \frac{1}{\sqrt{\varepsilon_0 \mu_0}} \cdot \vec{\nabla} \times \vec{H}$$
 (3)

$$\vec{D}(\omega) = \varepsilon_r(\omega) \cdot \vec{E}(\omega) \tag{4}$$

$$\frac{\partial \overrightarrow{H}}{\partial t} = \frac{-1}{\sqrt{\varepsilon_0 \mu_0}} . \overrightarrow{\nabla} \times \overrightarrow{E}$$
 (5)

In electromagnetic theory, (D) denotes the electric displacement or electric flux density, (H) represents the magnetic field intensity, and (E) signifies the electric field. The Finite-Difference Time-Domain approach presents insights into across both frequency and time scales, allowing for calculations of electromagnetic fields across time and frequency. In solving Maxwell's formulas for solar cell simulations under the AM 1.5G spectrum, parameters such as relative permittivity $\epsilon_r(\omega)$, or refractive index $n(\omega)$ and extinction coefficient $k(\omega)$, are necessary, with the magnetic permeability μr assumed to be one. The modeling process initiates with an initial electric field E_0 and progresses in time steps of 0.002 femtoseconds (fs), with the spatial volume discretized into small cells, minimizing cell size to 0.002 nm where rapid refractive index changes occur. Perfectly matched layer (PML) boundary conditions are applied along the Z-axis to absorb waves, while periodic boundary conditions are used for X and Y directions, reflecting the plasmonic elements's periodicity.

Upon solving Maxwell's formulas inside each Yee cell, the Poynting vector is determined to find the light power absorbed by comparing incident and outgoing waves. Electrical simulations then involve voltage steps and meshing at the 300 K temperature during operation, with Ohmic boundary conditions at the solar cell contacts to allow charge carrier flow. Reflecting boundaries are applied to the cell's sides to keep charge carriers within the simulation region. For current density calculations, drift-diffusion and nonlinear Poisson formulas are computed using device data from Table 2, carrier types, and concentrations. The drift-diffusion equations, fundamental for modeling carrier transport in semiconductors [30], are solved to determine the current density and electric potential. These formulas explain the movement of electrons and holes under the influence of electric fields and concentration gradients.

$$\vec{\nabla} \cdot \left(\mu_n \cdot \vec{\nabla} n - q D_n \cdot \vec{\nabla} p \right) + G - R = 0 \tag{6}$$

$$\vec{\nabla} \cdot \left(\mu_p \cdot \vec{\nabla} p - qD_p \cdot \vec{\nabla} n\right) - G + R = 0 \tag{7}$$

In these formulas, n and p denote the electron and hole carrier densities, respectively. μ_n and μ_p represent the mobilities of electrons and holes, while D_n and D_p are the diffusion coefficients for electrons and holes. The symbol q stands for the elementary charge, G is the carrier generation rate, and R indicates the recombination rate [30]. The Poisson formula can be expressed as:

$$\vec{\nabla} \cdot (\varepsilon \vec{\nabla} \Phi) = -\rho / q \tag{8}$$

In this equation, ε denotes the material's relative permittivity, Φ indicates the electrostatic potential, and ρ is the charge density [30]. The current density can be determined according to the following formula:

$$\vec{J} = q \left(n\vec{E}\mu_n + p\vec{E}\mu_p \right) \tag{9}$$

In this formula, q represents the elementary charge, µn and µp denote the mobilities of electrons and holes, n and p indicate the electron and hole carrier densities, and E is the electric field [30.]

Optical analysis techniques, such as absorption modeling, play a vital role in solar cell research as they allow scientists to analyze how light interacts with the materials within the cell. This information is crucial for improving solar cell efficiency and for designing new materials that can boost energy conversion. In the following part, we will discuss optical characterization in further depth.

3. RESULT AND DISCUSSION

Researchers analyze the absorption curve (Figure 2) to optimize materials and configurations photovoltaic devices. This curve shows how much light is absorbed across different wavelengths, helping determine the cell's power potential. Ideally, a solar cell should absorb as much light as possible across the solar spectrum, requiring a high absorption coefficient. Figure 2 highlights that for a basic cell (without nanostructures), absorption is limited in certain regions (1000-1150 nm), suggesting potential for improvement. Material engineering, such as integrating light-trapping structures like plasmonic nanostructures, can address these gaps by enhancing absorption in underperforming spectral regions. The absorption curve in Figure 2 also examines the effects of nanostructure size, material type, shape, and position on absorption within the active layer. In this

setup, the CIGS absorber layer surrounds plasmonic nanostructures, which affect the refractive index depending on their placement and material. Without these nanostructures (in a reference "bare" cell), the CIGS layer maintains a constant refractive index that varies only with the wavelength. The "bare" cell shows maximum absorption between 500-1000 nm. Absorption peaks and dips in the curve result from two main phenomena: scattering and plasmonic resonances. Metal nanostructures act as scattering centers, redirecting light within the cell, enhancing absorption by trapping light in the active material. However, scattering can also reduce absorption if light is scattered outside the cell. At specific wavelengths, localized surface plasmon resonances (LSPR) or surface plasmon polaritons (SPP) occur when light couples with the electron oscillations in the nanostructures, increasing absorption. However, when nanostructures are large or closely spaced, they may cause parasitic losses, reducing efficiency. The figure below shows the absorption spectrum as a function of wavelength for the samples. The increase in absorption compared to the simple cell has mostly occurred at wavelengths above 1000 nanometers. As observed in the figure, the highest absorption increase is related to Sample 3.

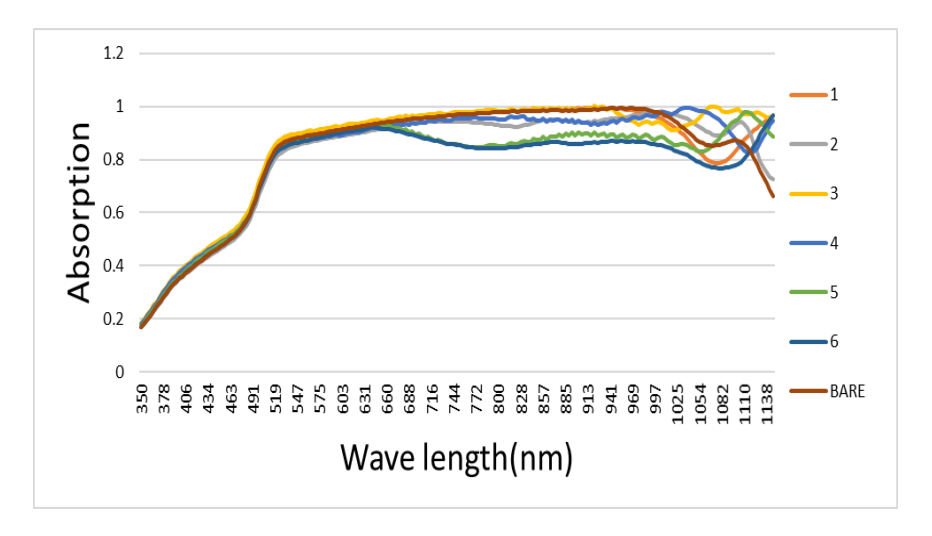


Fig. 2. Absorption spectrum of the cell with plasmonic nanostructures

The samples with nanostructures on the top of the CIGS layer show the most notable decrease in absorption due to light scattering outside the cell. The maximum efficiency achieved in this study (25.13% for Sample 5) is competitive with recent reports on CIGS cells enhanced by plasmonic nanostructures. For instance, Londhe et al. [10] reported an efficiency

enhancement using Au nanoparticles, and Hasheminassab et al. [18] investigated the influence of Ag nanoparticle shape. Our findings, particularly the high efficiencies observed for Au-based single elements (25.28% - 25.61%), align with the expectation that noble metals like Au and Ag provide superior plasmonic effects compared to Al [9, 15, 18]. This comparison underscores the effectiveness of the optimized configurations explored in this work.

Electrical characterization is crucial for assessing the efficiency of photovoltaic devices and optimizing their design for better energy efficiency. In this section, we focus on the outcomes of electrical characterizations, particularly through current-voltage (I-V) curves and the analysis of key parameters such as short-circuit current, open-circuit voltage, fill factor, and power conversion efficiency. Figure 3 highlights the effects of plasmonic elements on the I-V curve. These elements can encrease the current-voltage characteristics by improving energy absorption in the photoactive layer. The scattering and concentration of light lead to a higher generation rate of electronhole pairs, thus increasing the photocurrent. Furthermore, plasmonic nanostructures generate localized electromagnetic fields that assist in separating electron-hole pairs and reducing carrier recombination rates, which can improve both open-circuit voltage and fill factor. These improvements contribute to a more efficient solar cell, as evidenced by better performance in the I-V curve. The enhanced light absorption due to plasmonic nanostructures is often coupled with an increase in the generation of electron-hole pairs and improved current generation. However, factors like scattering, parasitic absorption, and resistance can counteract these benefits, leading to a reduced short-circuit current and potentially lower efficiency. The electrical response of the photovoltaic cell, therefore, relies on carefully balancing these effects to optimize charge carrier collection, recombination rates, and overall power output. The figure below presents the current-voltage (I-V) curves for the samples, highlighting their performance characteristics. It is evident from the data that all the samples show a significant improvement in electrical properties when compared to the simple solar cell. This enhancement results from the optimized placement of plasmonic structures within the absorber layer, leading to improved light confinement and enhanced charge carrier generation. These advancements indicate that integrating cubic and spherical nanostructures positively influences the overall energy conversion efficiency and performance of photovoltaic devices across different configurations.

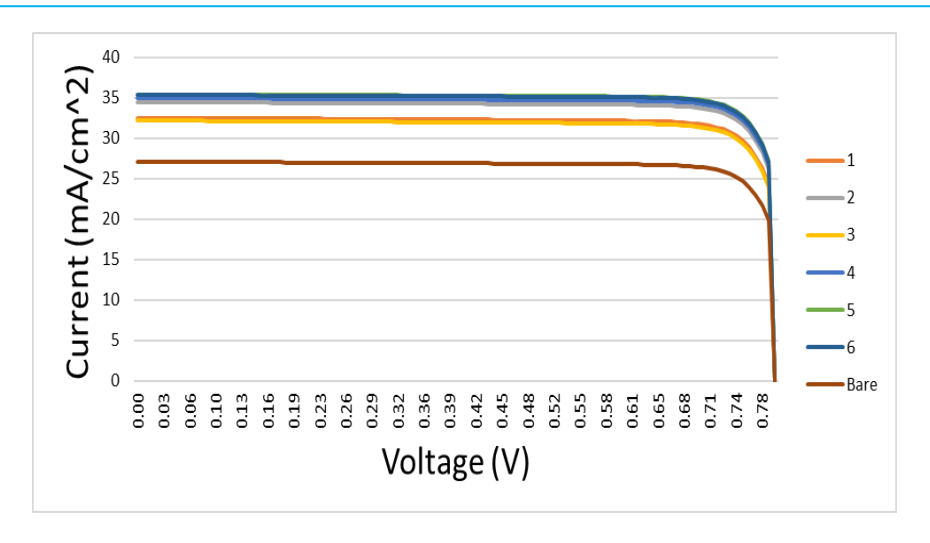


Fig. 3. I-V curve under the influence of plasmonic nanostructures

The table below provides the optical and electrical parameters for each sample. The optical parameter includes absorbed power in the modeled volume (P), while the electrical parameters include short-circuit current density (J), open-circuit voltage (V), fill factor (FF), and overall cell efficiency. Among the samples, Sample 5 demonstrates the highest efficiency increase of 25.13%. Table 3 details the simulated performance of the specific six dual-structure configurations (Samples 1-6) as defined in the Introduction. The efficiencies represent the combined effect of the two distinct nanostructures within each specific sample configuration.

	Table 3.	The electrical	and option	cal properties	of the samples
--	----------	----------------	------------	----------------	----------------

	P (Watts)	J(mA/cm ²)	Voc(V)	Pmax(mW/cm ²)	FF	Efficiency (%)
1	4.13E-11	32.5544	0.815603	22.8817	0.815603	22.88
2	4.04E-11	34.4695	0.867616	24.3706	0.814899	24.37
3	4.22E-11	32.2042	0.860843	22.6372	0.816558	22.63
4	4.10E-11	34.9951	0.86914	24.7626	0.814142	24.76
5	3.94E-11	35.4453	0.870598	25.1342	0.814496	25.13
6	3.86E-11	35.3713	0.87037	25.0763	0.814533	25.07

This significant improvement (for Sample 5) can be attributed to enhanced absorption within the wavelength range of 1000 nm, as shown in Figure 2. The specific arrangement of spherical nanoparticles at the top and cubic nanoparticles at the bottom likely provides complementary optical benefits. Spherical nanoparticles at the front interface are effective scatterers, redirecting incident light into the absorber layer and increasing the path length, particularly

for longer wavelengths where CIGS absorption is lower. Concurrently, cubic nanoparticles positioned near the back interface (Mo contact) may facilitate enhanced back-scattering or near-field interactions, redirecting light that has traversed the absorber layer for a second pass. This synergistic effect of frontincoupling and rear-recycling maximizes overall light trapping and absorption within the CIGS layer. Additionally, the electrical parameters of Sample 5, such as higher short-circuit current density (Jsc = 35.45 mA/cm²) and a favorable fill factor (FF = 0.814), contribute to its superior performance. As a result, Sample 5 achieves a marked efficiency boost compared to the simple solar cell (which has an efficiency of 19.03%) as well as the other samples. This highlights the effectiveness of its design in optimizing both optical and electrical performance. While plasmonic nanostructures enhance light trapping, they can also introduce parasitic losses that counteract these benefits. These losses primarily arise from 1) Ohmic losses within the metallic nanoparticles, where absorbed light energy is converted to heat rather than contributing to photocurrent generation, and 2) Scattering losses, where light is scattered out of the device structure or into nonabsorbing layers rather than being trapped within the CIGS absorber. These detrimental effects are particularly relevant for configurations with high nanoparticle occupancy surfaces (O.F.) or large particle sizes, as seen in Table 1, where high O.F. (0.64) was sometimes used for spherical elements, potentially increasing both scattering and ohmic losses. The optimization process implicitly balanced the beneficial light-trapping effects against these potential losses by varying size, shape, material, and O.F. The fact that Sample 3, despite incorporating potentially high-scattering elements, showed lower efficiency (22.63%) compared to Sample 5 (25.13%) or even the baseline cell (19.03%) suggests that its specific configuration may have suffered more significantly from such parasitic losses, possibly due to unfavorable scattering directions or excessive metal coverage. A more detailed examination reveals that these detrimental parasitic effects are particularly pronounced in configurations with high nanoparticle occupancy factors (O.F.) or large particle sizes, as indicated by the parameters explored in our optimization (Table 1). For instance, Sample 3 utilizes spherical nanoparticles with a high O.F. of 0.64, which likely increases both scattering and Ohmic losses, counteracting the beneficial light-trapping effects and resulting in lower efficiency than the baseline.

To mitigate these negative effects in our optimized designs, our study inherently employed a systematic approach during the optimization process. By varying key parameters such as size, shape, material, position, and occupancy factor (O.F.), we implicitly balanced the beneficial light-trapping effects against potential parasitic losses. The successful configuration of Sample 5 (spherical Au NPs at the top with O.F. 0.16 and cubic Au NPs at the bottom with O.F.

0.16) likely represents an optimized balance, minimizing excessive metal coverage while maximizing useful scattering. The placement of spherical nanoparticles at the front interface (low O.F.) effectively scatters incident light into the absorber layer, while the rear cubic nanoparticles (also low O.F.) may facilitate beneficial back-scattering, minimizing overall losses.

Furthermore, our analysis and comparison showing that single plasmonic nanostructures can achieve comparable efficiencies (up to 25.61%) with simpler fabrication implicitly demonstrates a practical strategy: opting for simpler, single-element designs to inherently reduce the complexity and potential for parasitic losses associated with dual configurations, thereby improving cost-effectiveness and manufacturability.

4. CONCLUSION

While plasmonic effects enhance light absorption and carrier generation, they also introduce challenges such as parasitic (ohmic and scattering) losses, which can reduce the short-circuit current and overall efficiency if not carefully managed. The design process involved balancing these competing effects through optimization of nanostructure properties (size, shape, material, position and occupancy surface) to maximize net efficiency gains. Careful material selection and optimization of plasmonic structure properties are essential to achieving the best performance. CIGS-based solar cells have gained attention for their cost-effective manufacturing and superior efficiency compared to traditional silicon-based solar cells. Their performance advantages, such as better performance under low light and compatibility with bendable substrates, position CIGS photovoltaic devices as a promising technology for future solar energy uses. This article explores the use of plasmonic nanostructures to further improve the efficiency of these cells. Plasmonic effects can boost light absorption, improve exciton generation and separation, and reduce recombination, all contributing to enhanced solar cell performance. The effect of plasmonic nanostructures on solar cells depends on factors such as the nano element size, shape, arrangement, and material composition. Simulations of the optoelectrical characteristics were performed, including absorption curves along with current-voltage characteristics and efficiency. Sample 5, featuring spherical elements at the top and cubic elements at the bottom, demonstrated the highest efficiency (25.13%) among these dual configurations. While this efficiency is slightly lower than the best single-element configurations, the investigation provides valuable insights into the comparative performance landscape of combined geometries versus individual ones. Although single plasmonic nanostructures (achieving up to 25.61% efficiency) offer comparable performance with potentially simpler fabrication, exploring dual configurations

helps understand the limits and potential synergies of combined geometries. The findings suggest that for the specific parameters and configurations explored, the benefits of dual integration may not significantly outweigh the advantages of simpler single-element approaches. This approach not only yields efficiencies that are comparable to those of more complex configurations but also provides significant benefits in terms of cost-effectiveness and simplification of the manufacturing process. While integrating two series of plasmonic nanostructures can further enhance light absorption, it introduces additional complexities, such as increased fabrication costs and technical challenges in aligning the nanostructures. Therefore, utilizing a single plasmonic nanostructure strikes a better balance between performance optimization and practical feasibility, making it a more efficient and cost-effective strategy for solar cell production. This finding underscores the potential of single-series plasmonic nanostructures in advancing solar technology while maintaining manufacturability.

Acknowledgment

The authors declare that no funds, grants, or other support were received during the preparation of this manuscript.

REFERENCES

- [1]. Machkih, Karima, Rachid Oubaki, and Mohammed Makha. *A Review of CIGS Thin Film Semiconductor Deposition via Sputtering and Thermal Evaporation for Solar Cell Applications*. Coatings 14.9 (2024): 1088. https://www.mdpi.com/2079-6412/14/9/1088
- [2]. Ramanujam, Jeyakumar, and Udai P. Singh. *Copper indium gallium selenide based solar cells–a review*. Energy & Environmental Science 10.6 (2017): 1306-1319. https://pubs.rsc.org/en/content/articlelanding/2013/ee/c7ee00826k/unauth
- [3]. Gohri, Shivani, Jaya Madan, and Rahul Pandey. *Augmenting CIGS solar cell efficiency through multiple grading profile analysis*. Journal of Electronic Materials 52.9 (2023): 6335-6349. https://link.springer.com/article/10.1007/s11664-023-10567-8
- [4]. Hashemi Nassab, Sayed Mohammad Sadegh, Mohsen Imanieh, and Abbas Kamaly. *The Effect of Doping and the Thickness of the Layers on CIGS Solar Cell Efficiency*. Journal of Optoelectronical Nanostructures 1.1 (2016): 9-24. https://sanad.iau.ir/en/Article/1182687
- [5]. Izadneshan, Heydar, Valery Gremenok, and Ghahraman Solookinejad. Fabrication of Cu (In, Ga) Se2 solar cells with In2S3 buffer layer by two stage process. Journal of Optoelectronical Nanostructures Summer 1.2 (2016). https://sanad.iau.ir/en/Article/1182669

- [6]. A. Mirkamali, K. K. Muminov, Numerical Simulation of CdS/CIGS Tandem Multi-Junction Solar Cells with AMPS-1D, Journal of Optoelectronical Nanostructures. 2(1) (2017) 31-40. https://jopn.miau.ac.ir/article_2198.html
- [7]. Royanian, Sahar, Ali Abdolahzadeh Ziabari, and Reza Yousefi. *Efficiency enhancement of ultra-thin CIGS solar cells using bandgap grading and embedding Au plasmonic nanoparticles*. Plasmonics 15.4 (2020): 1173-1182. https://link.springer.com/article/10.1007/s11468-020-01138-2
- [8]. Jacak, Janusz E., and Witold A. Jacak. *Plasmonic enhancement of solar cells efficiency: material dependence in semiconductor metallic surface nano-modification*. Plasmonics (2018). https://www.intechopen.com/chapters/62426
- [9]. ping, Sun. *Design of plasmonic nanoparticles for increasing efficiency and absorptance in thin-film solar cells*. Journal of Optics 53.1 (2024): 404-415. https://link.springer.com/article/10.1007/s12596-023-01180-3
- [10]. Londhe, Priyanka U., Ashwini B. Rohom, and N. B. Chaure. Improvement in the CIGS solar cell parameters by using plasmonic (Au) nanoparticle. Nanoscience and Nanotechnology 6.1A (2016): 43-46. https://engg.matoshri.edu.in/assets/pdf/science/achievements/2ABR/2.19.p df
- [11]. Abdolahzadeh Ziabari, Ali, et al. *Performance improvement of ultrathin CIGS solar cells using Al plasmonic nanoparticles: The effect of the position of nanoparticles.* Journal of Optoelectronical Nanostructures 5.4 (2020): 17-32. https://sanad.iau.ir/en/Article/1182858
- [12]. Rezvani, Masoud, and Maryam Fathi Sepahvand. *Simulation of surface plasmon excitation in a plasmonic nano-wire using surface integral equations*. Journal of Optoelectronical Nanostructures 1.1 (2016): 51-64. https://sanad.iau.ir/en/Article/1182690
- [13]. Bednar, Nikola, Noemi Severino, and Nadja Adamovic. *Optical simulation of light management in CIGS thin-film solar cells using finite element method*. Applied Sciences 5.4 (2015): 1735-1744. https://www.mdpi.com/2076-3417/5/4/1735
- [14]. Oliveira, António JN, et al. *Development of a Plasmonic Light Management Architecture Integrated within an Interface Passivation Scheme for Ultrathin Solar Cells*. Solar RRL (2024): 2400147. https://onlinelibrary.wiley.com/doi/full/10.1002/solr.202400147
- [15]. Waketola, Alemayehu G., Newayemedhin A. Tegegne, and Fekadu G. Hone. *Recent Progress in Silver and Gold Nanoparticle-Based Plasmonic Organic Solar Cells*. Plasmonics (2024): 1-36. https://link.springer.com/article/10.1007/s11468-024-02430-1

- [16]. Jeng, Ming-Jer, et al. *Improving efficiency of multicrystalline silicon and CIGS solar cells by incorporating metal nanoparticles*. Materials 8.10 (2015): 6761-6771. https://www.mdpi.com/1996-1944/8/10/5337
- [17]. Fjell, Mirjam D., et al. *Enhancing Silicon Solar Cell Performance Using a Thin-Film-like Aluminum Nanoparticle Surface Layer*. Nanomaterials 14.4 (2024): 324. https://www.mdpi.com/2079-4991/14/4/324
- [18]. Hasheminassab, S. M. S., et al. *Influence of the shape and size of Ag nanoparticles on the performance enhancement of CIGS solar cells: the role of surface plasmons.* Plasmonics 16.1 (2021): 273-282. https://link.springer.com/article/10.1007/s11468-020-01280-x
- [19]. Mann, Vidhi, and Vipul Rastogi. FDTD simulation studies on improvement of light absorption in organic solar cells by dielectric nanostructures. Optical and Quantum Electronics 52 (2020): 1-16. https://link.springer.com/article/10.1007/s11082-020-02328-2
- [20]. Ryu, Shinyoung, et al. Light intensity dependence of organic solar cell operation and dominance switching between Shockley–Read–Hall and bimolecular recombination losses. Scientific reports 11.1 (2021): 16781. https://www.nature.com/articles/s41598-021-96222-w
- [21]. Poh, Chung-How, et al. *FDTD modeling to enhance the performance of an organic solar cell embedded with gold nanostructures*. Optical Materials Express 1.7 (2011): 1326-1331. https://opg.optica.org/ome/fulltext.cfm?uri=ome-1-7-1326&id=223761
- [22]. Mulyanti, Budi, et al. *Absorption Performance of Doped TiO2-Based Perovskite Solar Cell using FDTD Simulation*. Modelling and Simulation in Engineering 2022 (2022). https://onlinelibrary.wiley.com/doi/full/10.1155/2022/9299279
- [23]. Eyderman, Sergey, and Sajeev John. Light-trapping and recycling for extraordinary power conversion in ultra-thin gallium-arsenide solar cells. Scientific reports 6.1 (2016): 28303. https://www.nature.com/articles/srep28303
- [24]. Rockstuhl, Carsten, Stephan Fahr, and Falk Lederer. *Absorption enhancement in solar cells by localized plasmon polaritons*. Journal of applied physics 104.12 (2008): 123102. https://pubs.aip.org/aip/jap/article-abstract/104/12/123102/557668/Absorption-enhancement-in-solar-cells-by-localized?redirectedFrom=fulltext
- [25]. Moliton, André, and Jean-Michel Nunzi. *How to model the behaviour of organic photovoltaic cells*. Polymer International 55.6 (2006): 583-600. https://scijournals.onlinelibrary.wiley.com/doi/abs/10.1002/pi.2038

- [26]. Benmir, A., and M. S. Aida. *Analytical modeling and simulation of CIGS solar cells*. Energy Procedia 36 (2013): 618-627. https://www.sciencedirect.com/science/article/pii/S1876610213011570
- [27]. Repins, Ingrid, et al. Required material properties for high-efficiency CIGS modules. Thin Film Solar Technology. Vol. 7409. SPIE, 2009. https://www.spiedigitallibrary.org/conference-proceedings-of-spie/7409/74090M/Required-material-properties-for-high-efficiency-CIGS-modules/10.1117/12.828365.short
- [28]. Weiss, Thomas P., et al. *Bulk and surface recombination properties in thin film semiconductors with different surface treatments from time-resolved photoluminescence* measurements. Scientific reports 9.1 (2019): 1-13. https://www.nature.com/articles/s41598-019-41716-x
- [29]. J.D. Jackson, *Classical Electrodynamics*, 3rd Edition, John Wiley & Sons, 1998.
- [30]. Sze, S.M., and Ng, K.K., *Physics of Semiconductor Devices*, 3rd Edition, John Wiley & Sons, 2006.